Journal of Power Sources 182 (2008) 270–277

Contents lists available at ScienceDirect

Journal of Power Sources

journal homepage: www.elsevier.com/locate/jpowsour

A three-phase current-fed dc/dc converter with a three-leg high frequency transformer for fuel cells

Hanju Cha [a,*], Jungwan Choi [b], Prasad Enjeti [c]

[a] Department of Electrical Engineering, Chungnam National University, 220 Gung-dong Yuseong-gu, Daejeon 305-764, Republic of Korea
[b] National Fusion Research Institute, Daejeon, Republic of Korea
[c] Texas A&M University, College Station, TX 77843-3128, USA

ARTICLE INFO

Article history:
Received 4 March 2008
Accepted 26 March 2008
Available online 1 April 2008

Keywords:
Three-phase dc/dc converter
Current-fed converter
Three-phase three-leg transformer
Zero-voltage switching
Leakage inductance
Fuel cells

ABSTRACT

In this paper, a three-phase current-fed dc/dc converter with an active clamp is introduced, and a new three-phase three-leg high frequency transformer is proposed for the converter. The three-phase dc/dc converter transfers power through transformer leakage inductances in the discontinuous current mode; a single common active clamp branch is employed for zero-voltage switching (ZVS) in all active switches. Further, the converter's three-phase power configuration increases power transfer, and it reduces the rms current per phase, thus reduces conduction losses. Moreover, a delta–delta connection on the three-phase transformer provides parallel current paths and reduces conduction losses in the transformer windings. A three-phase transformer can be constructed by connecting three discrete single-phase transformers, but this process results in a higher volume and higher material costs. Therefore, a new three-phase three-leg high frequency transformer is designed with three discrete cores integrated into a single transformer core. The proposed transformer is analyzed according to the several operating modes of the converter, and its design rules are determined. Experimental results are obtained on a 500-W prototype unit; the design is fully verified and analyzed.

1. Introduction

Fuel cells have been identified as a future source of clean energy and produce low-varying dc voltage in the range of 30–60 V. For stationary power applications, the power conditioning system for fuel cells consists of a low-voltage fuel cell as the primary source, a dc/dc converter to obtain isolated high voltage, and a dc/ac inverter to generate an ac voltage for commercial usages [1]. Since a dc/ac inverter supplies power to a 220-V ac utility, an isolated dc/dc converter is needed to convert low-varying dc voltage to a high, constant dc voltage of around 370 V [2]. Therefore, a high-power dc/dc converter with a high voltage transfer ratio is needed along with a transformer, which is usually employed for boosting voltage as well as for isolation. However, the high leakage inductance caused by the high turn-ratio in the transformer leads to trouble such as voltage spikes and electromagnetic noise. In order to achieve a high voltage transfer ratio while mitigating the effects of leakage inductance, a current-fed dc/dc converter with an active clamp has been introduced for single-phase applications [3,4].

Previous research has concentrated on the three-phase dc/dc converter due to its potential benefits, such as high power density and high-quality waveforms. However, most of the work thus far has been done on topology and PWM strategy for a voltage-fed dc/dc converter [5–8].

In this paper, a three-phase current-fed converter with an active clamp, capable of achieving high power application, is introduced. Major features of the converter include: a single common active clamp branch used for zero-voltage switching (ZVS) in all six active switches; three-phase power transferred in the discontinuous current mode through transformer leakage inductances, thus leading to zero current switching in rectifier diodes; and a single-phase current-fed dc/dc converter extended to the three-phase current-fed dc/dc converter, where a commonly used three-phase full bridge topology is employed. Some advantages are that with the converter the size of the input dc inductor is reduced and the output filter inductor is eliminated, and that the converter reduces conduction losses through distribution of rms current flowing through per-phase switches and transformer windings. Due to these advantages, this converter is highly suitable for use in the interface between a low-voltage high-power fuel cell source and an inverter load. It may also be used with another low-voltage renewable energy source such

* Corresponding author. Tel.: +82 42 821 7006; fax: +82 42 821 8895.
E-mail address: hjcha@cnu.ac.kr (H. Cha).

0378-7753/$ – see front matter © 2008 Elsevier B.V. All rights reserved.
doi:10.1016/j.jpowsour.2008.03.066

as a photovoltaic, which requires high-voltage, high-power dc/dc conversion.

A new three-phase three-leg high frequency transformer is designed for use with the aforementioned three-phase dc/dc converter. Analyses of operating modes and design rules for the transformer as well as the converter are addressed and confirmed through simulations. Experimental results for a 500-W prototype are provided to verify all the design rules and analyses.

2. Three-phase current-fed dc/dc converter

Fig. 1 shows a three-phase dc/dc converter with an active clamp. The three-phase dc/dc converter has outputs connected to a three-phase full-bridge diode rectifier through a delta–delta wound three-phase transformer. The three-phase dc/dc converter is divided into a three-phase full-bridge converter configured as six main MOSFET switches (S_1–S_6) (for three-phase dc/ac conversion), one auxiliary MOSFET switch (S_C) and a clamp capacitor (C_C) for the active clamp, and a dc boost inductor (L_{dc}) as a current source. The main switches and auxiliary clamp switch perform ZVS through the use of resonance between leakage inductances of the three-phase transformer and the sum of stray capacitors such as the clamp capacitor, output capacitances at MOSFET switches, and winding capacitances in the transformer. As a highly efficient, current-fed converter, it therefore reduces switching losses. It must be noted that the three-phase transformer can have the form of three discrete single-phase transformers connected in delta–delta winding, or of a three-leg transformer, as commonly used in the three-phase utility.

Fig. 2a shows a simplified circuit of the proposed three-phase dc/dc converter introduced in Fig. 1. The delta–delta wound three-phase transformer is represented by its three leakage inductances, L_{lk}, and its output voltage, V_O, on the secondary side, is referred to on the primary side as $V_O'(V_O' = V_O/n)$, where n is the turn-ratio of the transformer ($n = N_2/N_1$). Clamp capacitor C_C and output capacitor C_O are assumed to be infinite in value; these are replaced by voltage sources V_C and V_O, respectively. The boost inductor L_{dc} can be replaced by a constant current source, I_d, during each switching period. Fig. 2b shows ideal current waveforms of the boost inductor current I_d, phase A current i_A and clamp current i_{Sc}.

The sequence of topological states is described below in terms of Fig. 2b waveforms.

Before t_0: all six switches S_1–S_6 are turned on and the boost inductor L_{dc} charges energy from fuel cells V_d.

From t_0 *to* t_1: at t_0, switches S_2, S_3, S_4, and S_5 are turned off, but S_1 and S_6 are left on. The bridge voltage v_{PN} reaches the clamp capacitor voltage V_C and the clamp diode, which is the body diode of MOSFET S_C, conducts the boost inductor current I_d. The current through the leakage inductance L_{lk} increases as a slope determined by voltage difference between the clamp voltage V_C and the reflected output voltage V_O', as shown in (1). Phase A current I_A then starts flowing to the output. To facilitate ZVS for S_C, the clamp switch S_C is turned on before the clamp current i_{Sc} reverses at t_1. It should be observed that i_{Sc} is $-I_d$ at t_0, since $i_A(t_0) = 0$, and that it becomes zero at t_1.

$$i_A = \frac{V_C - V_O'}{(2/3)L_{lk}}t \tag{1}$$

$$i_{Sc} = -(I_d - i_A) \tag{2}$$

From t_1 *to* t_2: the clamp current i_{Sc} reverses its polarity and flows through MOSFET S_C. i_{Sc} provides the difference between the increasing i_A and constant boost inductor current I_d. Since expressions for i_A and i_{Sc} are the same as Eqs. (1) and (2) in this interval, i_{Sc} increases to I_d and i_A becomes $2I_d$ at t_2. i_{Sc} increases linearly from $-I_d$ to I_d for t_0–t_2, and clamp capacitor voltage V_C remains constant in the steady state because the charging energy for t_0–t_1 is the same as the discharging energy for t_1–t_2.

Maximum values of i_A and i_{Sc} are

$$i_{A(MAX)} = 2I_d = \frac{V_C - V_O'}{(2/3)L_{lk}}(1 - D)T_S \tag{3}$$

$$i_{Sc(MAX)} = -(I_d - i_{A(MAX)}) = I_d \tag{4}$$

From t_2 *to* t_3: at t_2, the active clamp switch S_C is turned off and the energy stored in L_{lk} discharges the output capacitances of S_3 and S_4, which are the upper and lower switch of S_6 and S_1, respectively. Then, v_{PN} decreases to zero voltage and the body diodes of S_3 and S_4 begin to conduct. Therefore all main switches, including S_3 and S_4, can be turned on under a zero voltage condition. i_A now decreases at a linear rate determined by the output voltage and the value of L_{lk}, as shown in the following equation:

$$i_A = i_{A(MAX)} - \frac{V_O'}{(2/3)L_{lk}}t \tag{5}$$

From t_3 *to* t_0': at t_3, i_A decreases to zero. All switches S_1–S_6 are on and boost inductor L_{dc} charges energy. At t_0', the four switches S_3, S_4, S_5, and S_6 are turned off, but S_1 and S_2 are left on. The input energy is transferred from fuel cells to the output capacitor C_O through the S_1–D_1–C_O–D_2–S_2 path. The same PWM scheme sequence is repeated for the S_1–S_2 switch pairs, as shown in Fig. 2b.

Clamp capacitor voltage in the steady state is determined using a voltage-second balance in the inductor L_{dc}. The formulas (6) and (7) represent ideal output voltage V_O and ideal clamp capacitor voltage V_C.

$$V_{O(ideal)} = \frac{nV_d}{1 - D} \tag{6}$$

$$V_{C(ideal)} = \frac{V_d}{1 - D} \tag{7}$$

The expression for real output voltage V_O is

$$V_O = \frac{n}{(1 - D)(1 + L_{lk}/L_m)}\left(V_d - \frac{2P_O(2/3)L_{lk}}{\eta V_d T_S}\right) \tag{8}$$

The real output voltage decreases from the ideal value in Eq. (6); this is mainly caused by leakage inductance L_{lk} and output power P_O. Therefore, leakage inductance L_{lk} reduces the overall voltage transfer ratio.

The expression for real clamp capacitor voltage V_C is

$$V_C = \frac{V_O}{n} + \frac{2(P_O/\eta V_d - I_m)(2/3)L_{lk}}{(1 - D)T_S} \tag{9}$$

where, I_m is the magnetizing current and

$$I_m = \frac{-V_O'(1 - D)T_S}{2L_m} \tag{10}$$

Real clamp capacitor voltage increases from the ideal value in Eq. (7) through the effect of leakage inductance L_{lk} and output power P_O; this means the maximum voltage stress on the clamp capacitor and the main switches increases as L_{lk} increases.

The minimum L_{lk} value necessary for ZVS to turn-on is

$$L_{lk} \geq \frac{(2V_dV_O/(1 - D)n - V_d^2/(1 - D)^2)C_S}{(P_O/\eta V_d + V_dDT_S/2L_{dc} + V_O(1 - D)T_S/2nL_m)^2} \tag{11}$$

where $C_S = C_{S_1} + C_{S_6} + C_{Sc}$ (in the interval of S_1–S_6).

The required L_{lk} for ZVS operation is determined by output power and switch stray capacitances. Fig. 3 shows that the minimum L_{lk} for ZVS decreases as output power P_O increases, which is a typical characteristic of soft switching converters. Leakage inductance L_{lk} must be greater than 100 nH for ZVS operation to occur, but

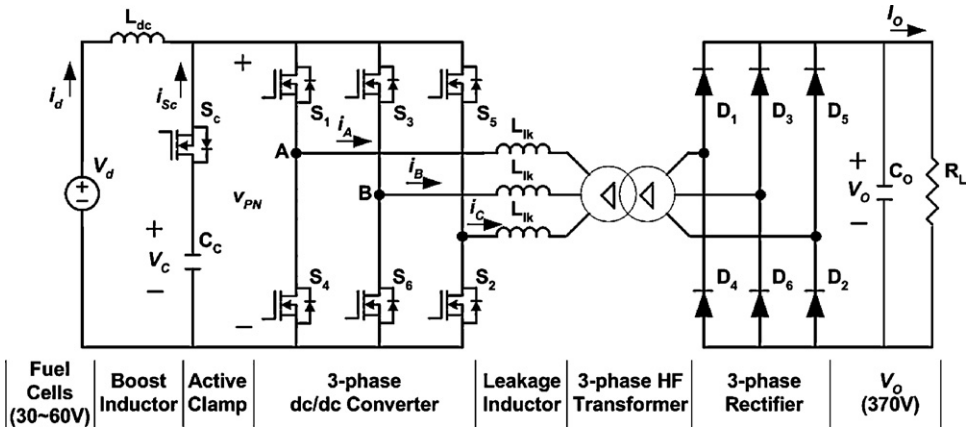

Fig. 1. Three-phase current-fed dc/dc converter.

needs to have a higher value still in order to reduce the peak $I_{A(MAX)}$, and thus to reduce rms current at the switches and transformer windings.

Fig. 4 shows simulation waveforms for output power $P_O = 500$ W, $V_d = 30$ V and $V_O = 370$ V, and the waveforms are obtained for the 25 kHz switching frequency ($T_S = 40$ μs), a 330-μH boost inductor L_{dc}, a 10 μH leakage inductance L_{lk}, and a three-phase transformer which has a 30-mH magnetizing inductance L_m and a 1:5 turn-ratio ($n = 5$). Fig. 4a shows boost inductor current I_d, which charges energy during DT_S and discharges energy during $(1-D)T_S$. Phase A current i_A, shown in Fig. 4b, flows with a typical waveform of 6-pulse operation to load the three-phase converter. In each 25 kHz switching period, only two switches are turned on in the sequence shown in Fig. 2b, and the paired on-switches repeat in the order of S_1–S_6, S_1–S_2, S_2–S_3, S_3–S_4, S_4–S_5, S_5–S_6, with variable duty. Fig. 4c shows the clamp capacitor current I_{Sc}, which forms six pulses of current in every three-phase cycle.

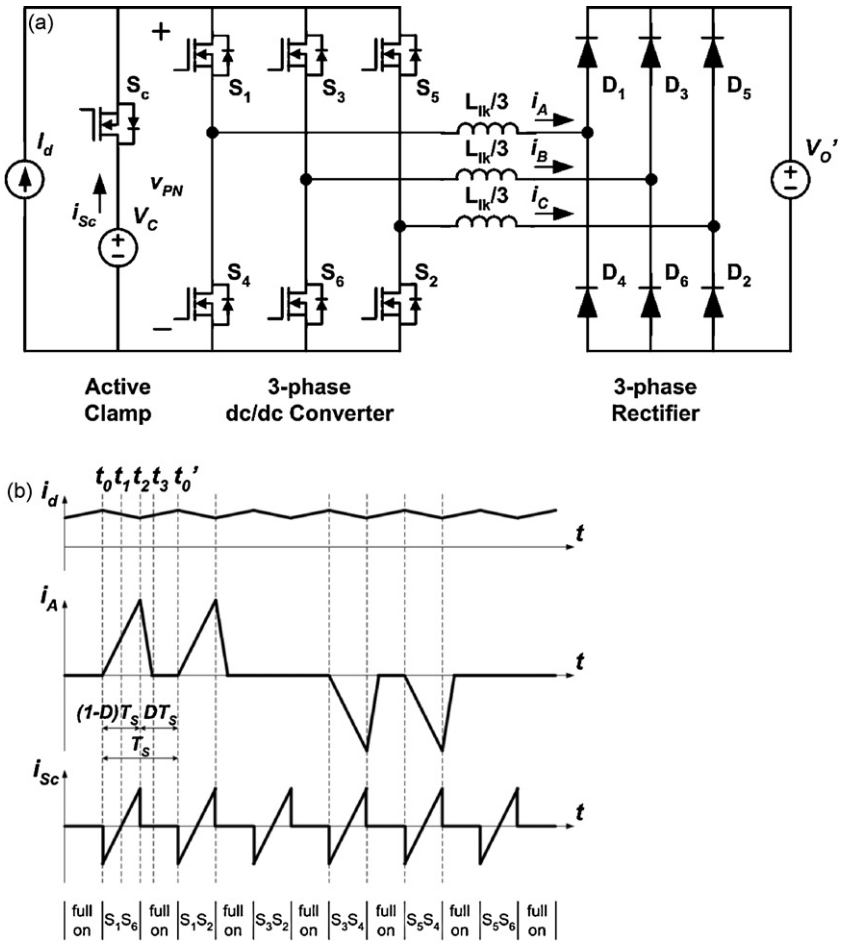

Fig. 2. (a) Simplified circuit of the three-phase dc/dc converter and (b) ideal waveforms of the proposed converter.

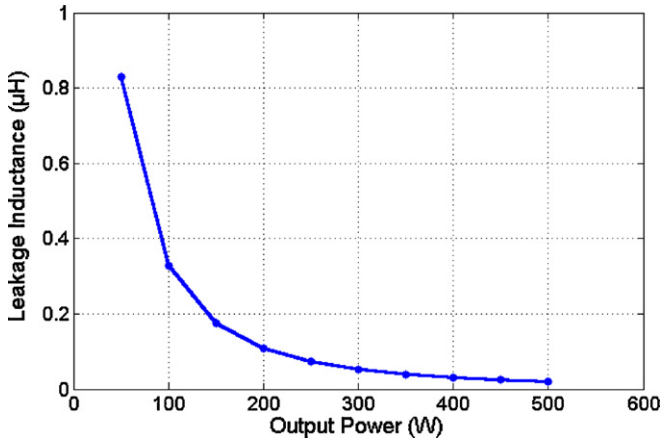

Fig. 3. Required L_{lk} for ZVS operation in terms of P_O.

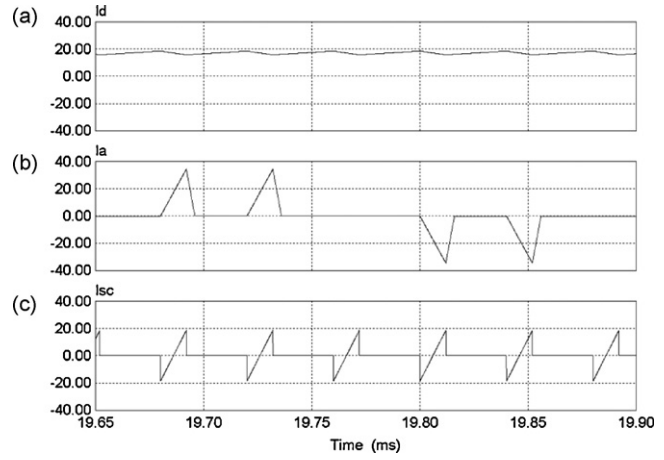

Fig. 4. (a) Boost inductor current I_d, (b) phase A current I_A (b) clamp current I_{Sc}.

3. Three-phase three-leg transformer design

Operating modes and current waveforms of the three-phase current-fed dc/dc converter were analyzed for designing a three-phase transformer; a three-phase three-leg transformer is preferable on account of its low volume and low material costs compared to three discrete single-phase high frequency transformers for high power application. Fig. 5 shows a delta–delta connected three-phase transformer, where L_m and L_{lk} represent magnetizing

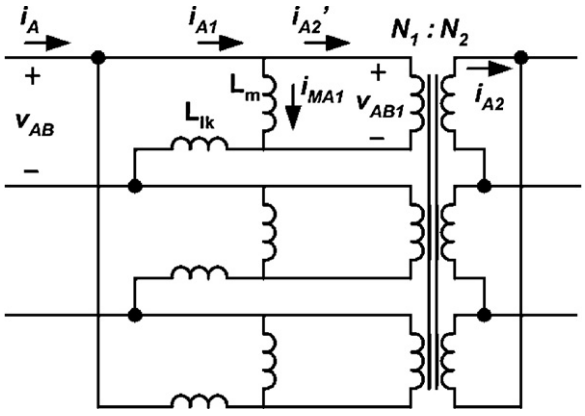

Fig. 5. Voltages and currents in the three-phase transformer.

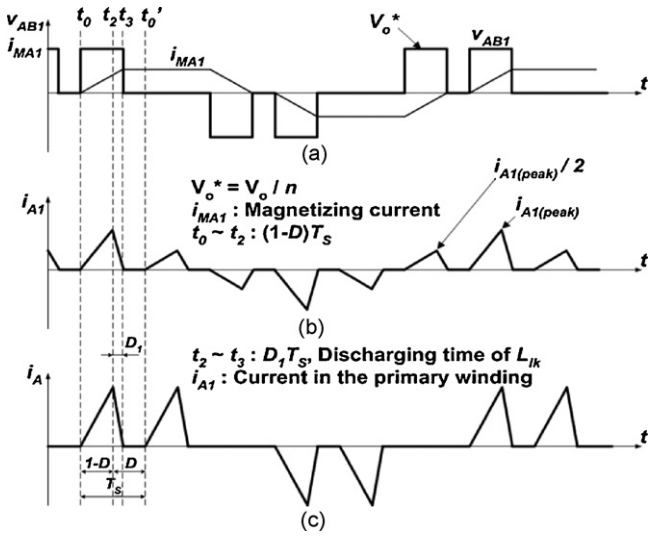

Fig. 6. (a) Primary voltage v_{AB_1} and magnetizing current i_{MA_1}, (b) primary winding current i_{A_1} and (c) converter output current i_A in phase A.

inductance and leakage inductance of phase A in the transformer. V_{AB}, i_A represent the phase A–B line-to-line voltage and phase A current in the dc/dc converter output, respectively, and v_{AB_1} and i_{A_1} represent the phase A–B line-to-line voltage and phase A current on the primary winding, respectively. Therefore, the phase current i_A from the dc/dc converter is the difference between i_{A_1} and i_{C_1}, which is $i_{A_1} - i_{C_1}$.

Fig. 6 shows voltage and current waveforms in the primary winding during phase A. As shown in Fig. 6a, the voltage v_{AB_1} is clamped by V_O', where V_O' is the reflected output voltage for the transformer's primary winding and v_{AB_1} does not include the voltage drop by the leakage inductance L_{lk}. The interval of each voltage pulse is the sum of $(1-D)T_S$ and corresponds to the discharging time for the energy stored in L_{lk}. The voltage waveforms consist of two positive voltage pulses and two negative voltage pulses, which have the same intervals. i_{MA_1} represents the magnetizing current flowing through L_m of phase A winding.

Fig. 6b shows a primary winding current i_{A_1}, which is the sum of magnetizing current i_{MA_1} and reflected secondary current i_{A2}' in phase A. Fig. 6c shows a converter output current i_A, which is equal to $i_{A_1} - i_{C_1}$. Fig. 6 shows that rms current of i_{A_1} in the primary winding is less than rms current of i_A because of delta–delta connection at the three-phase transformer.

Table 1 lists the operating conditions of the three-phase current-fed dc/dc converter; the three-phase three-leg transformer design was based on these conditions.

Design procedure for the transformer was addressed through the following.

3.1. Maximum flux linkage

The number of primary turns is determined by the voltage waveform applied to the primary winding and by parameters of the

Table 1
Operating conditions of the dc/dc converter

Converter circuit	3-Phase current-fed dc/dc converter
Turn ratio, n (N_2/N_1)	5
Operation frequency, f_s (kHz)	25
DC input voltage, V_d (V)	30
DC output voltage, V_O (V)	370
Output power, P_O (W)	500

core.

To determine the number of primary turns N_1, the following equation was used [9]:

$$N_1 = \frac{\lambda_1}{2\,\Delta B A_c} \times 10^4 \tag{12}$$

where

$$\lambda_1 = 2\int_{t_0}^{t_3} v_{AB_1}(t)\,dt \tag{13}$$

v_{AB_1} is the primary voltage across the magnetizing inductance and λ_1 is the maximum flux generated during the positive cycle of the primary voltage v_{AB_1}, as shown in Fig. 6a.

The maximum duty ratio D in the dc/dc converter was derived from Eq. (8), where L_{lk}/L_m was assumed to be a very small value and was disregarded.

$$D = 1 - \frac{n}{V_O}\left[V_d - \frac{2P_O}{\eta V_d}\frac{(2/3)L_{lk}}{T_S}\right] = 0.678 \tag{14}$$

In Fig. 6c, $D_1T_S = t_3 - t_2$ is the discharging time of the energy stored in the leakage inductance L_{lk}.

Variation in i_{A_1} at the rising interval in the positive voltage pulse was derived from Eq. (1), such that

$$\Delta i_{A_1} = \frac{V_C - V'_O}{L_{lk}}(1-D)T_S \tag{15}$$

Likewise, change in i_{A_1} at the falling interval was derived from Eq. (5), such that

$$\Delta i_{A_1} = \frac{-V'_O}{L_{lk}}D_1T_S \tag{16}$$

Since the absolute values of Eqs. (15) and (16) are equal, the value of D_1T_S can be calculated as follows:

$$D_1T_S = \left[\frac{V_d}{V'_O} - (1-D)\right]T_S = 3.34\,\mu s \tag{17}$$

Since the voltage waveform applied to the magnetizing inductance of the primary winding is the same as v_{AB_1} in Fig. 6a, λ_1 in (13) is equal to the area under the positive v_{AB_1} during $(1 - D + D_1)T_S$. As shown in Fig. 6a, the area is evaluated such that

$$\lambda_1 = 2V'_O[(1-D)T_S + D_1T_S] = 2.4 \times 10^{-3}\,V\,s \tag{18}$$

3.2. Core selection and shape modification

An EI-118 Ferrite core, made of the material PM_1 (Mn–Zn) and manufactured by ISU SERAMICS in Korea, is selected for this study. Since the EI-118 core is an EI core, a cross section of the center leg (leg B) is twice the area of both side legs (leg A and leg C). The width of the EI-118 core's center leg was 35 mm and the width of both side legs was 17.5 mm. In order to make the width of all three legs the same, both sides of the center leg were cut-out equally. Therefore, the width of the windows was increased by 8.75 mm in both directions. Fig. 7 shows the new form of the core after it was processed.

3.3. Parameters for the processed core

The original parameters were changed by cutting out the center leg, and the effective core area A_c was changed from 12.27 to 6.13 cm^2. Besides this, the window area was increased from 16.56 to 22.60 cm^2. No other parameter changes were considered in this design.

$$\text{modified } A_C = 6.13\,cm^2 \tag{19}$$

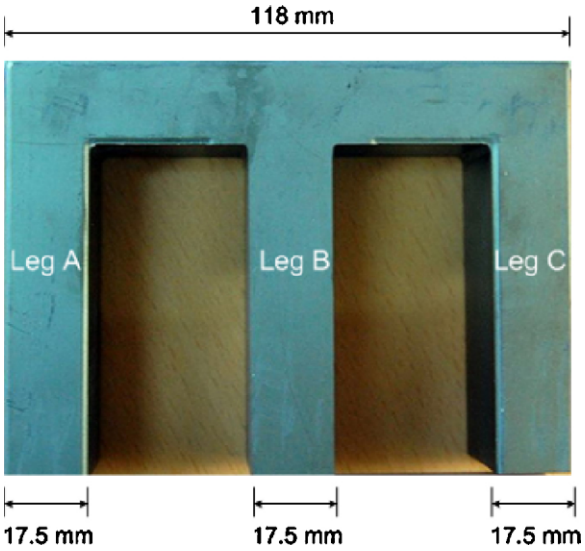

Fig. 7. Processed form of the core.

3.4. Number of primary turns

The EI-118 PM_1 Ferrite core from ISU CERAMICS has 0.34 T of saturation flux density at 100 °C. Therefore, the value of 0.19 T of ΔB was chosen. The core operates on the straight-line region of a hysteresis curve [10].

Primary turns N_1 was calculated by substituting Eqs. (18) and (19) and $\Delta B = 0.19$ T into Eq. (12)

$$N_1 = \frac{\lambda_1}{2\,\Delta B A_c} \times 10^4 = 10.3\,\text{turns} \tag{20}$$

So, a primary turns value of $N_1 = 15$ was chosen so as to leave a safety margin.

3.5. Wire selection

The leakage inductance of the three-phase transformer was set to 10 μH, and the peak value of i_{A_1} was obtained through Eqs. (15) and (16)

$$\Delta i_{A_{1(peak)}} = \frac{V_C - V'_O}{L_{lk}}(1-D)T_S = 24.7\,A \tag{21}$$

As shown in Fig. 6b, the rms current of the primary winding was obtained as follows:

$$I_{A_1} = i_{A_1(rms)} = \sqrt{\left[\left(\frac{i_A}{2}\right)^2 2 + i^2_{A_1(peak)}\right]}\frac{1-D-D_1}{3}\frac{1}{3} = 6.4A \tag{22}$$

If the allowed current density of copper wire is set to 4 A mm^{-2}, the cross-section area of the primary winding should be larger than 1.6 mm^2. Therefore, litz wire (which is formed from 235 individually insulated wires with diameters of 0.1 mm twisted together) was chosen. The total cross-section area of the litz wire was about 1.8 mm^2.

Since the rms value of the secondary current is one-fifth times that of the primary current, rms current at the secondary winding is 1.28 A, and the cross section area of the secondary winding should be larger than 0.32 mm^2. For implementation of the design, five wires of a 0.4-mm diameter were twisted together, with a cross-section area of about 0.63 mm^2.

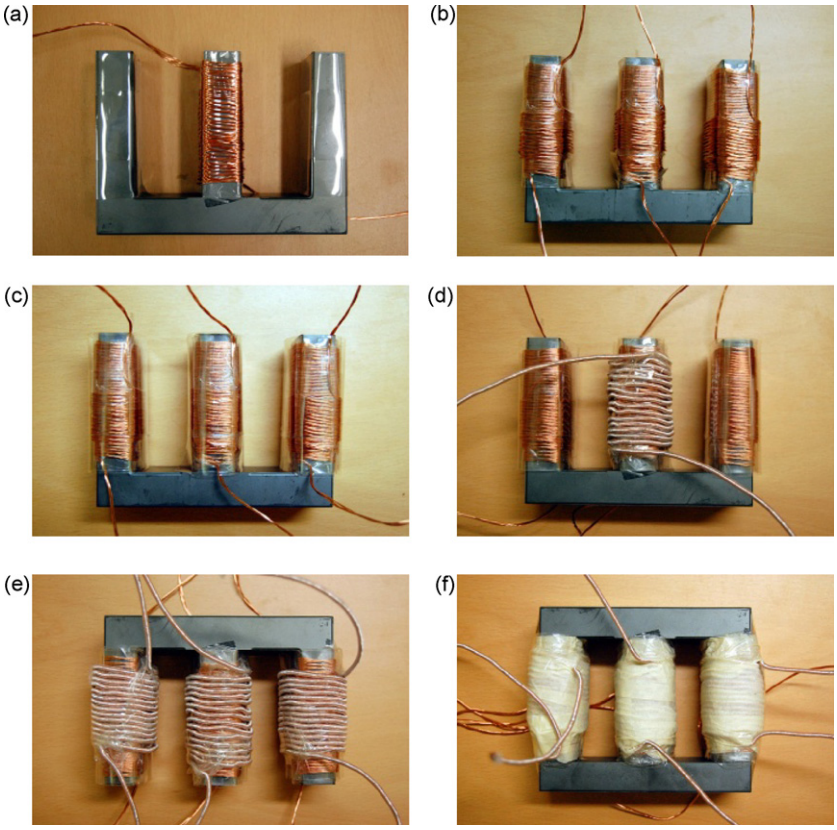

Fig. 8. Transformer assembly process (a–f).

3.6. Three-phase three-leg transformer assembly

The three-phase three-leg transformer was assembled by winding the secondary side first, then the primary side. Fig. 8 shows the assembly process for the transformer. Miler film was used for insulation between the layers.

3.7. Measured parameters of the transformer

Parameters of the transformer were measured with the HIOKI 3532-20 LCR HiTESTER, using a 25 kHz, 0.1 V test voltage. To measure the magnetizing inductance L_m, all the other windings of the transformer should be open, and should be short when measuring the leakage inductance L_{lk}. Table 2 shows the parameters measured.

Table 2
Transformer parameters measured by the LCR meter

	Leg A	Leg B	Leg C
L_{lk} (μH)	2.68	2.45	3.36
L_m (mH)	1.92	2.45	1.87

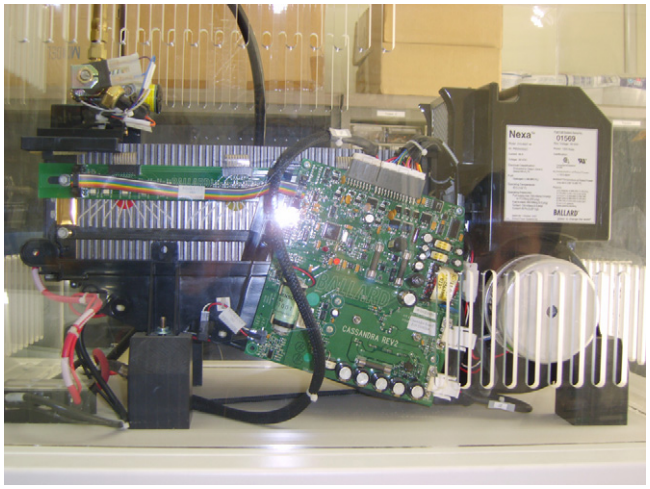

Fig. 9. 1.2 kW Ballard Nexa power module.

4. Experimental results

In the experimental prototype, an actual fuel cell (1.2 kW Ballard Nexa Power Module), which is displayed in Fig. 9, is implemented in order to test the proposed converter and the overall system performance under consideration of the nonlinear *V–I* characteristics

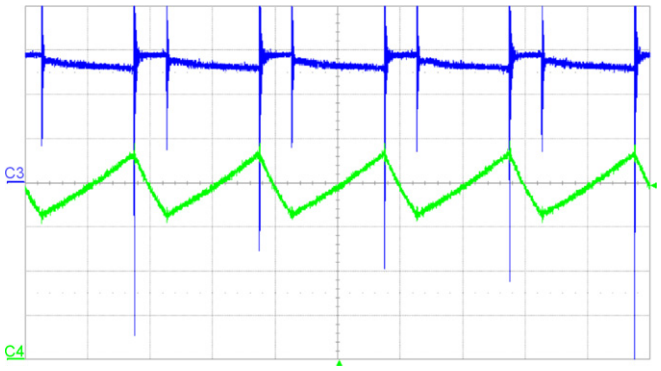

Fig. 10. Voltage and current waveform of the fuel cell stack (10 V div^{-1}, 5 A div^{-1}, 20 μs div^{-1}).

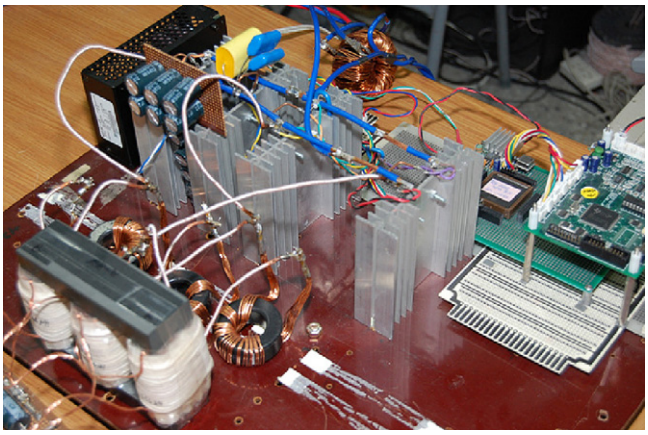

Fig. 11. 500 W prototype three-phase dc/dc converter with the three-phase transformer.

of the PEM fuel cell. Output voltage and current waveform from the PEM fuel cell stack are depicted in Fig. 10 with 30 V input voltage (V_d), 370 V output voltage (V_O), 500 W of input power (P_i) and duty $D = 0.76$

The leakage inductance of the transformer was set to 10 μH to ensure zero-voltage switching in the bridge switches and the clamp switch, and an adequate amount of rms current in the switches and transformer windings. Since the leakage inductance of the three-phase transformer was only about 2.5–3.4 μH, the 7.9 μH inductors were added externally and connected to the primary winding of the three-phase transformer in a series; this accounted for 10.7 μH of the total leakage inductance.

Fig. 11 shows a 500-W prototype three-phase current-fed dc/dc converter with the proposed three-phase three-leg high frequency transformer.

Fig. 12 shows the input dc current I_d, the primary voltage v_{AB_1}, the primary current i_{A_1}, the phase A current i_A and clamp capacitor current i_{Sc}. The experiment was carried out with a 30 V input voltage (V_d), a 370 V output voltage (V_O), 526 W of input power (P_i), and 489 W of output power (P_O). The efficiency of the converter was about 93%. A duty ratio D of 0.689 was selected to generate 371 V of output voltage; this duty ratio was the same value as that calculated in Eq. (14).

The experimental waveforms were in close accordance with the simulation results. Voltage and current waveforms measured in the proposed transformer were exactly the same as the waveforms of the three discrete single-phase transformers connected in delta–delta winding.

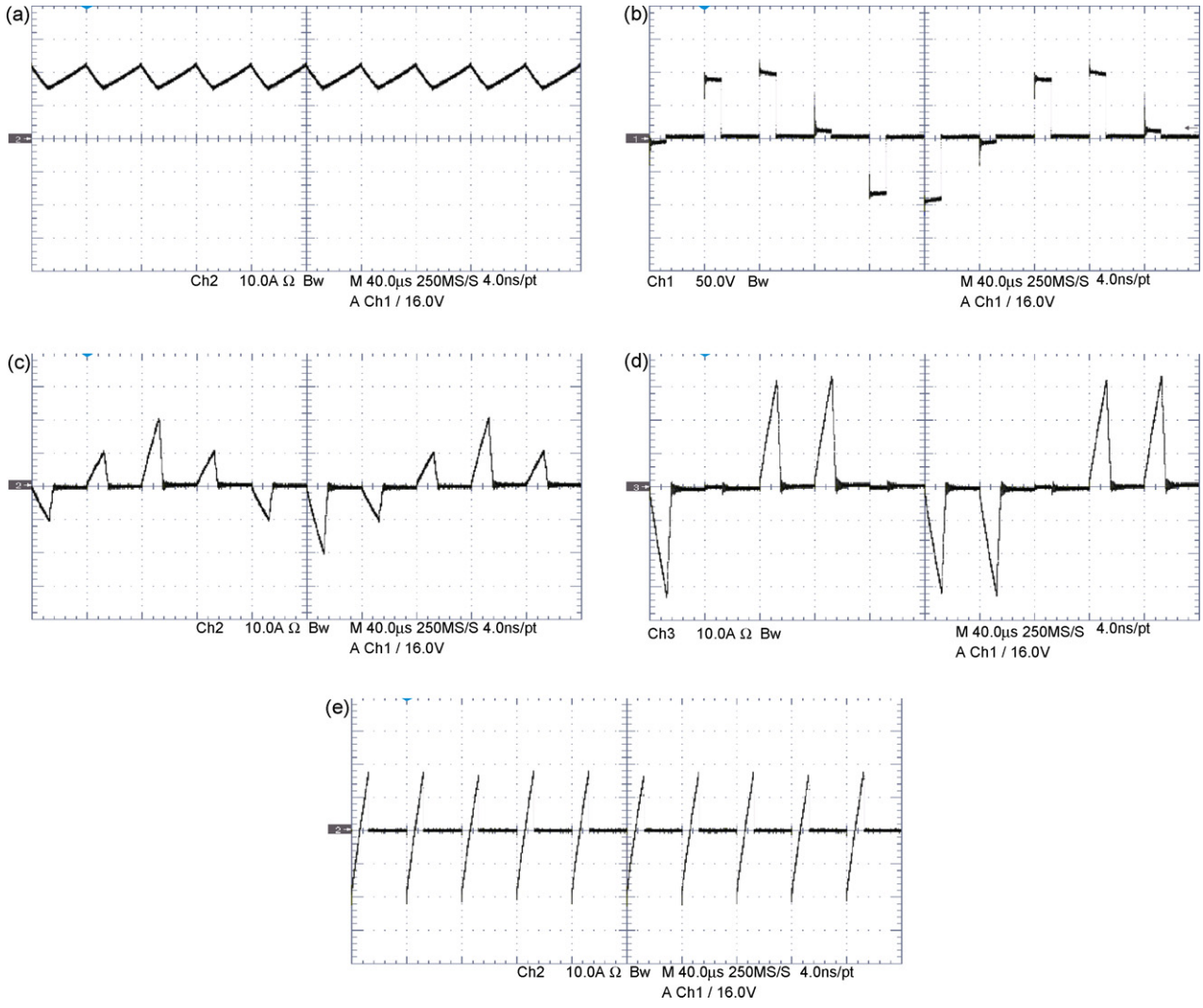

Fig. 12. (a) I_d (10 A div^{-1}), (b) v_{AB} (50 V div^{-1}), (c) i_{A_1} (10 A div^{-1}), (d) i_A (10 A div^{-1}), and (e) i_{Sc} (10 A div^{-1}).

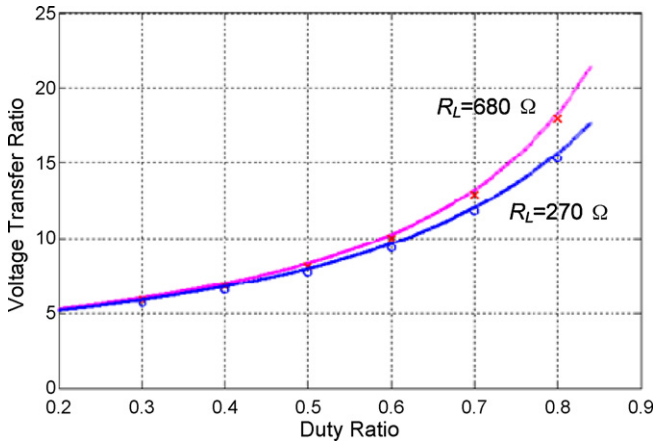

Fig. 13. Voltage transfer ratio.

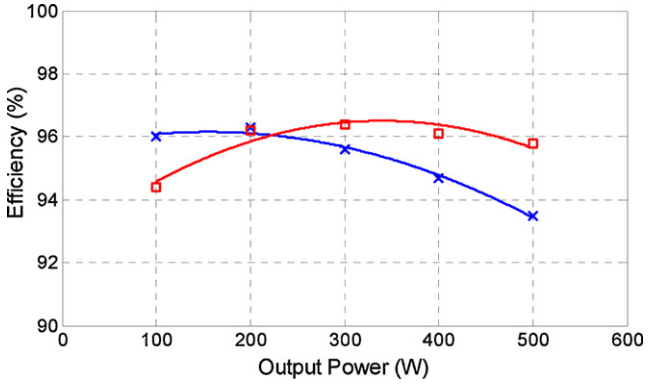

Fig. 14. Converter efficiency curves in V_d = 30 V (blue, "×") and 45 V (red, "□"). (For interpretation of the references to color in this figure legend, the reader is referred to the web version of the article.)

Fig. 13 shows curves for experimental and calculated voltage transfer ratio, as a function of duty ratio D and load. Voltage transfer ratio is defined as the ratio of output voltage V_O to the input voltage V_d. The experimental results match very closely with the output voltage calculated though Eq. (8), and reveal a significant influence of L_{lk} on the output voltage.

Zero-voltage switching in the active switches and zero current switching in the rectifier diodes improve converter efficiency. The curve in Fig. 14 shows measured efficiency curves for different loads while a 370 V output voltage is maintained and input voltage V_d is 30 and 45 V, respectively. The efficiency curve in 45 V of V_d shows better performance because an increased input voltage causes currents to decrease, and thus conduction losses in the converter decrease as well.

5. Conclusion

In this paper, a three-phase current-fed dc/dc converter with an active clamp has been introduced, and an overview has been provided on the process in which a three-phase three-leg high-frequency transformer was analyzed, designed, assembled and tested. The converter showed a high efficiency (of above 93%). This high efficiency can be accounted for not only by the zero-voltage switching in all active switches through use of a common active clamp branch, but also through zero current switching in the rectifier diodes by means of discontinuous current conduction. Further, the converter's power transfer is increased due to its three-phase power configuration and it reduces the rms current per phase, thus reduces the conduction losses, as well. Moreover, a three-phase three-leg high frequency transformer has been designed and three discrete cores have been integrated into a single transformer core. The three-phase transformer provides parallel current paths and reduces conduction losses in the transformer windings. These advantages make this converter suitable for high efficiency, high power applications with renewable energy sources such as fuel cells and photovoltaic. Finally, experimental results have been obtained through a 500 W prototype unit, with all of the design having been fully verified and analyzed.

Acknowledgement

This work has been supported by KESRI(R-2007-1-015-03), which is funded by Ministry of Knowledge Economy.

References

[1] M.W. Ellis, M.R. Spakovsky, D.J. Nelson, Proc. IEEE 89 (12) (2001) 1808–1818.
[2] D.K. Choi, B.K. Lee, S.W. Choi, C.Y. Won, D.W. Yoo, J. Power Sources 152 (2005) 245–255.
[3] W.C.P. De Aragao Filho, I. Barbi, Proceedings of the Telecommunications Energy Conference, 1996, pp. 313–320.
[4] K. Wang, L. Zhu, D. Qu, H. Odendaal, J. Lai, F.C. Lee, Proceedings of the Power Electronics Specialists Conference, 2000, pp. 1058–1063.
[5] A.R. Prasad, P.D. Ziogas, S. Manias, IEEE Trans. Ind. Appl. 28 (1992) 824–832.
[6] D. de Souza Oliveira, I. Barbi, IEEE Trans. Power Electron. 20 (2) (2005) 370–377.
[7] J. Jacobs, A. Averberg, R. De Doncker, Proceedings of the Power Electronics Specialists Conference, 2004, pp. 1861–1867.
[8] C. Liu, A. Johnson, J. Lai, IEEE Trans. Ind. Appl. 41 (2005) 1691–1697.
[9] R. Erickson, D. Maksimovic, Fundamentals of Power Electronics, 2nd ed., University of Colorado, 2001.
[10] A. Pressman, Switching Power Supply Design, 2nd ed., McGraw-Hill, New York, 1998.